JOURNAL OF SPACECRAFT AND ROCKETS
Vol. 29, No. 3, May-June 1992

Free-Flight Trim-Angle Predictions for the Aeroassist Flight Experiment

Leslie A. Yates* and Ethiraj Venkatapathy*
Eloret Institute, Palo Alto, California 94303

The aerodynamic coefficients and trim angle for an aerobrake at Mach numbers of 9.2 and 11.8 were found using a combination of experiment and computation. Free-flight tests were performed at NASA Ames Research Center's Hypervelocity Free-Flight Aerodynamic Facility, and the forebody pressure distribution was calculated using a three-dimensional Navier-Stokes code with an effective specific heat ratio. The computed drag, lift, and moments were used to prescribe the number of terms in the aerodynamic coefficient expansions and to specify values of the higher-order terms, and the experimental aerodynamic coefficients and trim angle were extracted from the experimental data. The experimental and computed aerodynamic coefficients and trim angles were in good agreement. The trim angle obtained from the free-flight tests, 14.7 deg, differed from the design trim angle, 17 deg, and from the Langley wind-tunnel results, 12 deg in air and 17 deg in CF_4. These differences are attributable to real-gas effects.

Nomenclature

A	= reference area
C_D, C_L, C_M, C_N, C_Y	= aerodynamic coefficients for the drag, lift, moment, yaw, and side forces, respectively
C_j	= undetermined parameter
C_{ps}	= stagnation pressure coefficient
f_{calc}	= function representing calculated position or orientation of the model
f_{exp}	= function representing experimental position or orientation of the model
I_x, I_y, I_z, I_{xz}	= moments of inertia
l	= reference length
m	= mass
p, q, r	= roll, pitch, and yaw rates, respectively, of the body axes
p_w, q_w, r_w	= angular rates of the wind axes
R	= ratio of base pressure to the stagnation pressure
t	= time
V	= velocity
w_i	= weighting function
x, y, z	= model coordinates
x_E, y_E, z_E	= Earth-fixed coordinate system
α, β	= pitch and yaw angles, respectively
γ	= specific heat ratio
$\Delta\zeta$	= offset parallel to base of the center of gravity
ρ	= freestream density
σ^2	= standard deviation
ϕ_w, θ_w, ψ_w	= angles defining the direction of the wind axes

Introduction

THE design of hypersonic transports, advanced space transportation systems, the Aeroassist Flight Experiment (AFE), and the Mars sample return mission requires accurate determination of aerodynamic coefficients and trim angles. Presently, chemically reactive computational fluid dynamics (CFD) codes and ideal-gas CFD codes with constant, effective specific heat ratios γ provide drag and lift coefficients adequate for the design of a variety of configurations. For flows in thermochemical equilibrium and for ideal-gas flows, CFD codes have also matched experimental moment coefficients and trim angles for some configurations. For example, moment coefficients for the AFE that were calculated using an inviscid, equilibrium-air solver matched those obtained in wind tunnels.[1,2] However, for flows in thermochemical nonequilibrium, the ability of CFD codes to predict actual moment coefficients and trim angles has been questioned,[3] and experiments that either simulate flight conditions or that can be used for validation of real-gas codes are still required for accurate determinations of the trim angle.

One facility that can be used either to simulate flight conditions or to provide data for validation of real-gas codes is the Hypervelocity Free-Flight Aerodynamic Facility (HFFAF) at NASA Ames Research Center. In the HFFAF models are in free flight and the amplitude of the pitching motion can be large. Since the aerodynamic coefficients are highly nonlinear in angle of attack for many of the configurations tested in the HFFAF, higher-order terms in the coefficient expansions cannot be ignored. These terms can be accurately identified if there are multiple runs with more than one cycle of motion and if the amplitude of the motion varies from run to run. However, because of time constraints on the facility and difficulties in designing models with the desired aerodynamic characteristics, it is not always possible to meet these criteria. If they are not met, the data reduction techniques will find aerodynamic coefficients that, on the average, are correct. However, individual terms in the expansions will not be correct.

For trim angle studies the higher-order terms in the moment-coefficient expansions must be correct. As will be demonstrated later, a suitable expansion of the moment coefficient for the range of motion of the AFE models tested in the HFFAF is

$$C_M = C_{M_\alpha} \sin(\alpha - \alpha_{\text{trim}}) + C_{M_\alpha^2} \sin^2(\alpha - \alpha_{\text{trim}})$$

where α is the angle of attack and α_{trim} the trim angle. The curvature of the function that describes the moment coefficient is given by $C_{M_\alpha^2}$. For the cases illustrated in Fig. 1 the curvature term has been fixed at -0.06, 0.00, and 0.06. With the curvature fixed the data reduction procedure adjusts both the trim angle and C_{M_α} to obtain the best possible fit to the data. As illustrated in Fig. 2, this can result in a large shift in

Presented as Paper 91-1632 at the AIAA 22nd Fluid Dynamics, Plasma Dynamics, and Lasers Conference, Honolulu, HI, June 24-26, 1991; received Aug. 10, 1991; revision received Jan. 21, 1992; accepted for publication Jan. 26, 1992.

*Research Engineer, NASA Ames Research Center, MS 230-2, Moffett Field, CA 94305. Member AIAA.

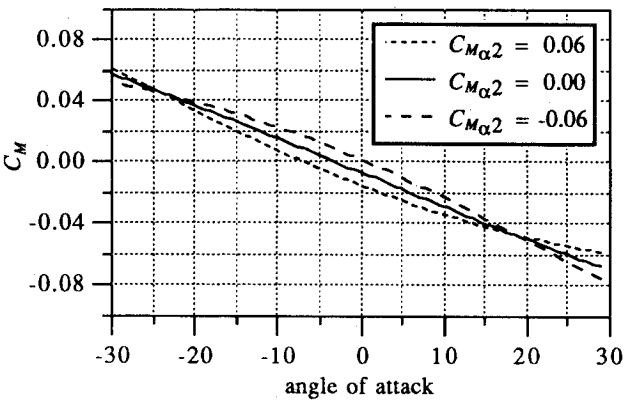

Fig. 1 Moment coefficient for fixed curvature.

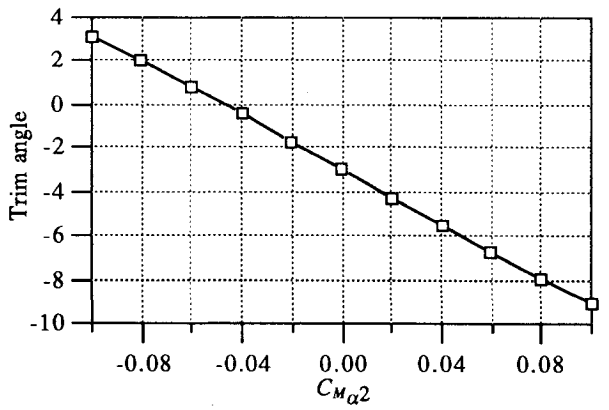

Fig. 2 Trim angle vs $C_{M_\alpha 2}$.

Table 1 Experimental conditions

Run	Pressure, Torr	Temperature, K	Velocity, km/s	Mach number	x_{cg}, in.[a]	z_{cg}, in.[a]
1700	19.6	297	3.3	9.2	0.059	0.008
1701	15.0	296	4.1	11.8	0.059	0.008

[a]Measured from center of the base plane.

the calculated trim angle. The trim angle changes from 3.2 deg to − 9.0 deg when the curvature changes from − 0.1 to 0.1. This range is too large to be acceptable for vehicle design.

In 1987 HFFAF studies of the AFE,[4] linearized equations of motion were used in the data reduction procedures and the predicted trim angle was 22 deg. This value is much larger than both the value of the design trim angle obtained from Newtonian calculations (17 deg) and the value from wind-tunnel results (12 deg) (Ref. 5). Linearizing the equations of motion limits the Taylor series expansions of the aerodynamic coefficients to first order in angle of attack, and any effects of the curvature of the moment coefficient on the trim angle are ignored. As shown in Figs. 1 and 2, this could partially account for the discrepancy between the free-flight trim angle and the design and wind-tunnel trim angles.

The AFE free-flight data[4] that are suitable for aerodynamic analysis are very limited, and there is not enough information for the six-degree-of-freedom procedure to accurately resolve the higher-order terms in the coefficient expansions. These data, however, do contain valuable information necessary for AFE design. To extract this information, experimental analysis is used in conjunction with CFD. By use of ideal-gas computations with an effective γ, aerodynamic coefficients are calculated. These calculated coefficients are then used to prescribe the number of terms in the aerodynamic coefficient expansions and to fix the higher-order terms in the expansions. The six-degree-of-freedom procedure is then used to find the lower-order terms and trim angles, and the CFD and experimental results are compared.

Model Description

The AFE is an aerobrake design composed of geometrical shapes: an ellipsoidal nose tangent to a 60-deg half-angle elliptical cone that is raked at a 73-deg angle. The model has a base skirt with the base plane at a 17-deg angle relative to the body axis.[6] A sketch of the scale model of the AFE tested in the HFFAF tests is shown in Fig. 3.

In HFFAF studies of the AFE, runs 1700 and 1701 (Ref. 4) were suitable for aerodynamic analysis. The freestream conditions and model center of gravity locations for these two runs are given in Table 1. For both runs the models had an AFE forebody fabricated from aluminum and a screw afterbody for holding the model in the sabot during launch. At the symmetry plane, the base diameter of the model was 0.73 in. The measured offset of the center of gravity from the design center of gravity was small (Δx = 0.009 in. and Δz = − 0.008 in.); these measurements are accurate to ± 0.001 in. Each run had the model in view for 15 of the 16 shadowgraph stations. There were almost two complete cycles of motion, and the amplitude of the motion ranged between ± 33 deg from design trim. No roll pins were included on this model, and the roll and roll rates were deduced from the pitching and yawing motion.

Experimental Data Analysis

The HFFAF can duplicate Reynolds numbers, Mach numbers, and enthalpies experienced in hypersonic flight. The freestreams are known and uncontaminated, and the projec-

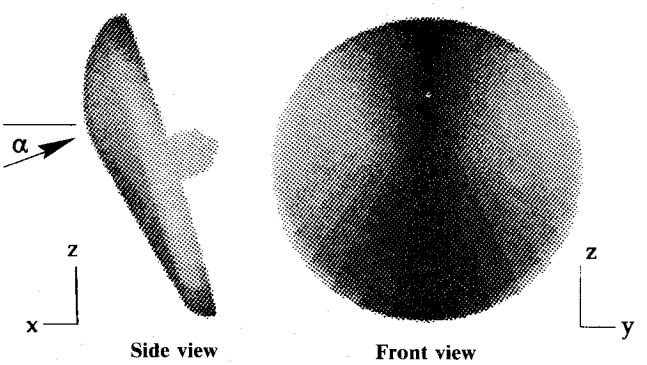

Fig. 3 Sketch of the AFE model.

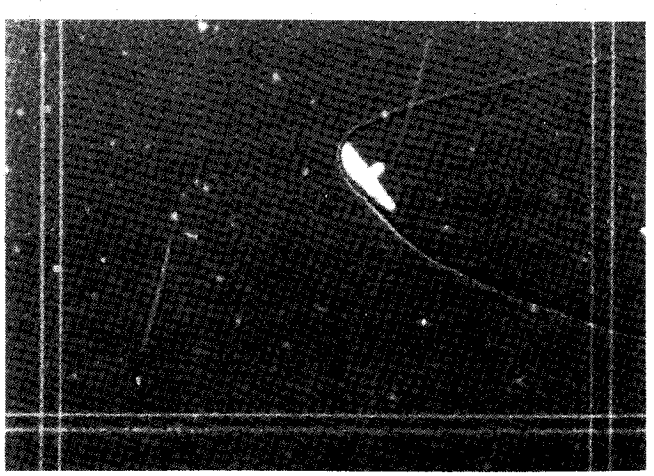

Fig. 4 Shadowgraph of the AFE model.

tiles are in free flight; hence, there are no sting effects and the base flows are realistic. The test times are short, and since the models are small and generally not recoverable, remote instrumentation is used. For aerodynamic studies, orthogonal shadowgraphs are taken of the model as it flies down the facility; a representative shadowgraph is shown in Fig. 4. In the HFFAF there are 16 shadowgraph stations, and the time at which the model arrives at each station is known to ± 5 ns. The three-dimensional orientation and position of the model are obtained from the shadowgraphs, and the aerodynamic coefficients are found using a six-degree-of-freedom, weighted, least-squares procedure that fits calculated trajectories to the measured orientations and positions of the model.

The trajectory of a free-flight model with an axis of symmetry can be described by 11 coupled, first-order, nonlinear, differential equations[7] written in Earth, wind, and body coordinate systems:

Earth axes:

$$\dot{x}_E = V \cos\theta_w \cos(\psi_w) \tag{1}$$

$$\dot{y}_E = V \cos\theta_w \sin(\psi_w) \tag{2}$$

$$\dot{z}_E = V \sin\theta_w \tag{3}$$

Wind axes:

$$\dot{V} = -(\rho A V^2/2m) C_D \tag{4}$$

$$\dot{\phi}_w = p_w + [q_w \sin\phi_w + r_w \cos\phi_w] \tan\theta_w \tag{5}$$

$$\dot{\theta}_w = q_w \cos\phi_w + r_w \sin\phi_w \tag{6}$$

$$\dot{\psi}_w = [q_w \sin\phi_w + r_w \cos\phi_w] \sec\theta_w \tag{7}$$

Body axes:

$$\dot{\alpha} = q - q_w \sec\beta - [p\cos\alpha + r\sin\alpha] \tan\beta \tag{8}$$

$$\dot{\beta} = r_w \sec\beta + p\sin\alpha - r\cos\alpha \tag{9}$$

$$I_y\dot{q} = \tfrac{1}{2}\rho A l V^2 C_M + I_{zx}(r^2 - p^2) + (I_z - I_x) rp \tag{10}$$

$$I_z\dot{r} = \tfrac{1}{2}\rho A l V^2 C_N + I_{zx}(p - qr) + (I_x - I_y) pq \tag{11}$$

where

$$p_w = [p\cos\alpha + r\sin\alpha]\cos\beta + (q - \dot{\alpha})\sin\beta \tag{12}$$

$$q_w = (\rho A V/2m) C_L \tag{13}$$

$$r_w = -(\rho A V/2m) C_Y \tag{14}$$

Coriolis and gravity terms, though not shown here, have also been included in the equations of motion. The differential equation for roll (p) has been omitted, and p is assumed to be of the form

$$p = p_0 + p_1 t + p_2 t^2 + \cdots \tag{15}$$

Generally, the aerodynamic coefficients are expanded in $\sin\alpha$ $\cos\beta$ and $\sin\beta$ (the crossflow velocity terms divided by the total velocity; p, q, and r (the angular rates); and $\dot{\alpha}$ and $\dot{\beta}$ (Refs. 7 and 8). For run 1700 the model roll was minimal and the yawing motion was less than a few degrees. For run 1701 the model was both rolling and yawing; however, since so few experimental data exist and computations for yawed models were not performed at these conditions, it had to be assumed that yaw and roll had little effect on the pitching moment and that pitch and roll had little effect on the yawing moment. Furthermore, since $q \approx \dot{\alpha}$ and $r \approx \dot{\beta}$, these terms cannot be separated, and only q and r are used in the coefficient expansions. For this study the coefficient expansions are of the following form:

$$C_M = \sum C_{M_{\alpha^n}} [\sin(\alpha - \alpha_{\text{trim}})\cos\beta]^n + C_{M_q} q \tag{16}$$

$$C_N = \sum C_{N_{\beta 2n+1}} \sin^{2n+1}\beta + C_{N_r} r \tag{17}$$

$$C_D = C_{D_0} + \sum C_{D_{\alpha^n}} [\sin(\alpha - \alpha_{\text{trim}})\cos\beta]^n + \sum C_{D_{\beta 2m+1}} \sin^{2m+1}\beta \tag{18}$$

$$C_L = C_{L_0} + \sum C_{L_{\alpha^n}} [\sin(\alpha - \alpha_{\text{trim}})\cos\beta]^n \tag{19}$$

$$C_Y = \sum C_{Y_{\beta 2n+1}} \sin^{2n+1}\beta \tag{20}$$

In the six-degree-of-freedom program the trajectory of the model is calculated using the nonlinear differential equations [Eqs. (1–11)] and the expansions for the aerodynamic coefficients [Eqs. (16–20)]. The initial conditions, roll, roll rate, and each term in the coefficient expansions are estimated. A weighted, least-squares procedure[8] is then used to find corrections for these estimates. These corrections are found as follows. First, the square of the residual (SSR) is written as

$$\text{SSR} = \sum_{i=1}^{N} w_i \left[f_{\text{exp}}(t_i) - f_{\text{calc}}(t_i) - \sum_j \left(\frac{\partial f}{\partial C_j}\right)_i \Delta C_j \right]^2$$

where the summation is over all of the data points, w_i is the weight, C_j are the undetermined parameters including initial conditions, f_{calc} is the calculated value of the model orientation or position using the equations of motion and the best estimate for the parameters, and $\partial f/\partial C_j$ is found by differentiating the equations of motion with respect to C_j and integrating. By use of standard least-squares analysis, the square of the residual is differentiated with respect to the ΔC_j, the resulting equations are set to zero, and the ΔC_j are found by solving the matrix equation

$$\boldsymbol{A}\,\Delta C = \boldsymbol{B}$$

where

$$A_{j,k} = \sum_{i=1}^{N} w_i \left(\frac{\partial f}{\partial C_j}\right)_i \left(\frac{\partial f}{\partial C_k}\right)_i$$

$$B_j = \sum_{i=1}^{N} w_i \left(\frac{\partial f}{\partial C_j}\right)_i [f_{\text{exp}}(t_i) - f_{\text{calc}}(t_i)]$$

The corrected parameters are then used in the equations of motion, and the process is repeated until the corrections are less than some specified value.

In the data analysis procedure it is possible to fix one or more terms in the coefficient expansions. In this study the free-flight data for the AFE were very limited, and the second- and higher-order terms in the expansions of the drag, lift, and moment coefficients could not be determined accurately. In the data analysis procedure the second- and higher-order terms were fixed by CFD computations. The zeroth- and first-order terms and the trim angle were found using the least-squares procedure. Discrepancies in the experimental and computed aerodynamic coefficients and trim angle would manifest themselves in differences in these low-order terms.

The estimated errors for the coefficients and for functions of these coefficients are readily available from the least-squares analysis and the quality of the fit.[9] For example, assuming randomly distributed errors and a very simple expansion for the drag coefficient,

$$C_D = D_{D_0} + C_{D_\alpha} \sin\alpha$$

the error in the experimental drag coefficient is given by $\sqrt{\text{VAR}(C_D)}$, where

$$\text{VAR}(C_D) = \text{VAR}(C_{D_0}) + 2\text{COV}(C_{D_0}, C_{D_\alpha}) \sin\alpha + \text{VAR}(C_{D_\alpha}) \sin^2\alpha$$

The variance (VAR) and covariance (COV) terms are

$$\text{VAR}(C_i) = A_{i,i}^{-1}\sigma^2 \quad \text{and} \quad \text{COV}(C_i, C_j) = A_{i,j}^{-1}\sigma^2$$

The predicted error for the drag coefficient is a function of the variances for each term in the expansion of the coefficient, the covariances, and the angle of attack. Since the covariance terms can be negative, the minimum error does not necessarily occur at 0 deg. Instead, it typically occurs in the region where most of the data are clustered or in the vicinity of the root-mean-square angle. It should be noted that this error analysis does not include functional errors, i.e., errors resulting from using incorrect expansions of the aerodynamic coefficients.

Computations

In the HFFAF tests the angle of attack varied between -33 and $+33$ deg. Modeling the higher-order terms in the moment coefficient expansions requires similar angular ranges in the computed solutions and small increments between solutions. Five-degree increments were used in this study. The computer resources needed for these solutions can become quite extensive, especially if the entire configuration is considered.

The CPU requirements of currently available real-gas CFD codes are too large for this study. For the forebody alone, some of the three-dimensional nonequilibrium solvers[10,11] require on the order of 40 CPU hours for a single steady solution at a given angle of attack. Equilibrium gas solvers require less time; however, the CPU time for a single steady solution is still on the order of hours. If the afterbody is included in the computational domain, the required computer time for both the nonequilibrium and equilibrium gas solvers is even greater due to base flow complexities.

To reduce CPU requirements, a very efficient ideal-gas solver (FL3D) with an appropriate choice of γ has been used in this study to compute the forebody pressure distributions. FL3D is a three-dimensional Navier-Stokes solver based on Roe's approximate Riemann solver, and it has global, second-order spatial accuracy. The governing Navier-Stokes equations are integrated in time, and a steady solution is obtained through alternating direction implicit scalar tridiagonal inversions. The details of this numerical scheme are given in Refs. 12 and 13. The FL3D solver has been validated with experiments for a variety of hypersonic three-dimensional corner and nozzle-plume flows.[14,15] This application of the FL3D solver to three-dimensional, hypersonic blunt-body flows is new.

The computational grid is constructed using an algebraic grid generation program, and the outer boundary is chosen so that the shock surface remains well within the computational domain for all angles of attack considered in this study. The computational grid consists of 34 grid points along the body, 23 points in the circumferential direction, and 25 points between the body and outer boundary. Since no solutions with nonzero yaw angles are sought, only half of the physical domain is included and symmetry boundary conditions are used to simulate the complete flow. The grid between the body and outer boundary is relatively coarse. There are approximately seven points in the boundary layer, and the skin-friction forces are three to four orders of magnitude less than the pressure forces. Since the skin-friction forces are small, no attempt has been made to futher refine their contribution to the aerodynamic coefficients. It should be noted than an Euler solver would have been sufficient for this study. However, FL3D is a very efficient solver, and switching to an Euler solver would have provided only minimal reductions in CPU requirements.

The AFE forebody solutions require special treatment of the boundary condition along a singular line that coincides with the stagnation line at zero angle of attack. No other modifications of the solver were required. Various boundary extrapolation and averaging procedures were tried along the singular boundary, and most of these resulted in oscillatory solutions in the vicinity of this singular line.[16] For the present work the boundary procedure that eliminated the singular line and resulted in smooth solutions at all angles of attack is closely related to finite-volume boundary procedures.

In this procedure, a small cylindrical hole region is formed around the singular axis. Grid points placed on the surface of the hole region form the axis-boundary surface, the solution is not solved for inside the hole, and a computed solution from the interior of the computational domain is extrapolated to this boundary. Other boundary procedures and local transformations have also been investigated.[16]

In addition to the axis-boundary condition, isothermal, no-slip boundary conditions are applied at the wall; the wall temperature is equal to the freestream temperature. Extrapolated outflow boundary conditions are imposed on the outflow planes. At the outer boundary surface, freestream boundary conditions are applied.

Previous studies of blunt bodies (e.g., Refs. 17 and 18) have shown that the real-gas effects on the pressure distribution can be approximated using an equivalent ideal gas with an effective γ. This effective γ can be chosen either by comparing an ideal-gas solution with a real-gas solution, by comparing computed shock shapes with experimental shock shapes, or by matching the real-gas isentropic relationships for the density ratio across a normal shock.[19] In this study γ was initially chosen from shock tables,[20] and shock shape comparisons were then used to refine the estimate.

In Fig. 5 a shadowgraph of the AFE model and computational pressure contours for coarse grid solutions using $\gamma = 1.4$ and $\gamma = 1.2$ and a finer, adaptive grid solution using $\gamma = 1.2$ are shown. For the $\gamma = 1.4$ solution the distance between the computed bow shock and the surface is a factor of 2 too large. For the coarse grid, $\gamma = 1.2$ solution, there is extensive smearing of the shock; however, the experimental shock does lie within the computational shock width. Once the coarse grid solution was obtained, more grid points were added and SAGE,[21] a three-dimensional adaptive grid code, was used to cluster the grid points toward the shock. In the adapted grid solution the resolution of the shock is greatly improved, and its location is in excellent agreement with the experimental shock location. For these conditions an effective γ of 1.2 models the real-gas effects, and the binary scaling factor $\rho\Delta$ (where Δ is the shock standoff distance)[22] indicates that the flow is in equilibrium.

To further reduce the computational resource requirements, the base flow region was excluded from the computational domain. However, the pressure on the base region cannot be ignored. Studies have shown that the pressure on the base is nearly constant and is of the order of 4% of the stagnation pressure.[23] These corrections have been included in the aerodynamic computations.

For the test conditions for run 1700, flow solutions were computed for angles of attack between -30 and $+30$ deg for $\gamma = 1.2$; for run 1701 solutions were computed between -25 and $+25$ deg for $\gamma = 1.2$ and between -25 and $+30$ deg for $\gamma = 1.4$. To minimize CPU time, a steady solution was first

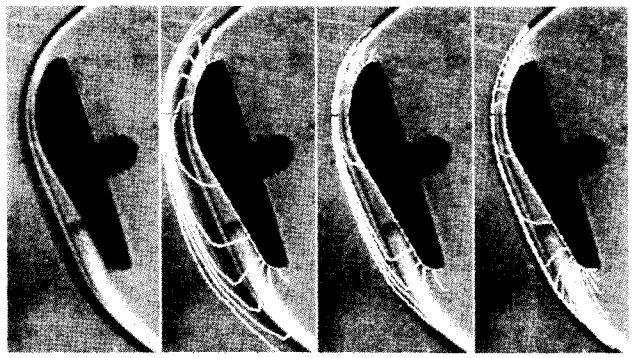

Fig. 5 Comparison of experimental and computed bow shock location.

obtained for 0-deg angle of attack and for one of the two freestream conditions. This first solution required 3000 time steps for convergence, or 1800 CPU seconds on a CRAY YMP. For additional flow solutions with differing Mach numbers, angles of attack, or γ, already computed solutions closest to the new conditions were used as starting solutions. This reduced the time requirements for the new solution by a factor of 10; only 180 CPU seconds were required for converged steady solutions. The FL3D solver is vectorized and has an efficiency of 2.5×10^{-5} CPU seconds per grid point per time step.

The computed surface pressure coefficients at the symmetry plane are plotted in Fig. 6 for coarse grid solutions with freestream conditions for run 1700. At negative angles of attack, the stagnation point is on the ellipsoidal nose, a pronounced peak in the pressure occurs at the stagnation point, and the peak pressure is much larger than that on the conical section of the forebody. As the angle of attack increases, the ratio of the peak pressure to the pressure on the conical section decreases until the stagnation point moves onto the conical section of the forebody. At all angles of attack, the pressure on the conical surface decreases as the distance from the ellipsoidal nose increases. The motion of the stagnation point and the change in the ratio of the stagnation pressure to the pressure on the conical surface cause nonlinearities in the aerodynamic coefficients.

Contour plots in the symmetry plane, on the surface, and in the base plane (not shown) indicate that the pressure coefficient along the conical section of the model decreases gradually, and the maximum pressure occurs in this region at large, positive angles of attack. In addition, there is a strong expansion at the base of the forebody, and at large positive and negative angles of attack there are appreciable circumferential pressure gradients.

The character of the pressure distribution on the conical section of the forebody for the $\gamma = 1.2$ adapted grid solution differs from that of the $\gamma = 1.2$ and $\gamma = 1.4$ coarse grid solutions. At a 5-deg angle of attack, the pressure at the transition from the ellipsoidal nose to the conical section for the two $\gamma = 1.2$ solutions is approximately the same. However, for the adapted grid case the pressure on the conical section is almost constant, whereas for the coarse grid solution it decreases gradually. The resulting drag, lift, and moment coefficients are larger for the adapted grid solution. Preliminary results indicate that the differences in the aerodynamic coefficients for the coarse and adapted grid solutions are on the order of the base flow corrections. However, the magnitude and sign of errors introduced by the relatively coarse grids are not known over the entire range of angles of attack, and these corrections have not been included in this study.

For the $\gamma = 1.4$ coarse grid solution the pressure at the transition point between the ellipsoidal nose and conical section of the forebody is larger than that for either the coarse or adapted grid $\gamma = 1.2$ solution. It decreases more rapidly than for either of the two $\gamma = 1.2$ cases, and the calculated drag, lift, and moment coefficients for the $\gamma = 1.4$ solution are not appreciably different from those for the $\gamma = 1.2$ coarse grid solution. This may change if adapted grids are used for both the $\gamma = 1.4$ and $\gamma = 1.2$ computations.

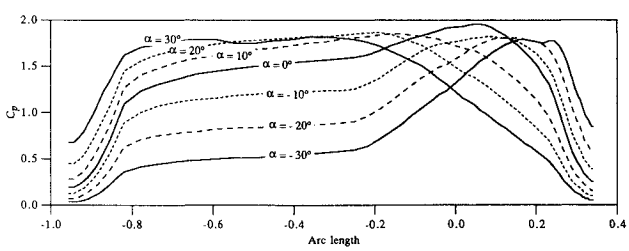

Fig. 6 Surface pressure coefficient on symmetry plane, conditions for run 1700, $\gamma = 1.2$.

Future computational work should include studies of the effects of the grid on the surface pressure distribution, especially in the conical section of the forebody. The forebody pressure distribution in this region can be sensitive to γ (refs. 1, 2, and 24) and to any variations in γ. At least one real-gas solution should be computed for these cases so that the effects of γ variations on the pressure distribution can be studied.

Aerodynamic Results

The pressure distribution on the forebody was integrated to give the computed drag, lift, and moment coefficients at various angles of attack. The computed trim angles were then calculated from the moment coefficients, and the aerodynamic coefficients were approximated by polynomials in $\sin(\alpha - \alpha_{\text{trim}})$. A least-squares analysis was used to calculate the value of each term in the expansions, and the expansions were truncated when the higher-order terms became small. For these runs, $\sin(\alpha - \alpha_{\text{trim}})$ reached a maximum value of 0.5, and several terms in the polynomial expansions had to be kept: three terms in the moment coefficient expansions (including trim angle) and four terms in the drag and lift coefficient expansions. The values of these terms are given in Table 2.

The corrections to these terms from the base pressure contribution are approximated by

$$\Delta C_D = -RC_{p_s} \cos(\alpha - 17 \text{ deg})$$

$$\Delta C_L = RC_{p_s} \sin(\alpha - 17 \text{ deg})$$

$$\Delta C_M = RC_{p_s} \Delta\zeta/l$$

where l is the reference length (base diameter). For models such as the AFE the average base pressure is approximately 4% of the stagnation pressure.[23] For all CFD computations

Table 2 Computed coefficients

	Run 1700, $\gamma = 1.2$	Run 1701, $\gamma = 1.2$
	Drag	
C_{D_0}	1.264 ± 0.004	1.246 ± 0.003
C_{D_α}	0.984 ± 0.022	0.905 ± 0.017
$C_{D_{\alpha 2}}$	-1.177 ± 0.034	-1.218 ± 0.028
$C_{D_{\alpha 3}}$	-0.807 ± 0.121	-0.662 ± 0.120
	Lift	
C_{L_0}	0.389 ± 0.003	0.371 ± 0.001
C_{L_α}	-0.713 ± 0.015	-0.732 ± 0.008
$C_{L_{\alpha 2}}$	-1.065 ± 0.022	-1.034 ± 0.014
$C_{L_{\alpha 3}}$	0.750 ± 0.080	0.847 ± 0.060
	Moment	
α_{trim}, deg	-1.74	-1.03
C_{M_α}	-0.153 ± 0.001	-0.151 ± 0.001
$C_{M_{\alpha 2}}$	-0.045 ± 0.003	-0.047 ± 0.003

Table 3 Experimental coefficients

	Run 1700	Run 1701
	Drag	
C_{D_0}	1.229 ± 0.004	1.278 ± 0.024
C_{D_α}	0.95 ± 0.042	0.84 ± 0.067
$C_{D_{\alpha 2}}$	-1.14 (fixed)	-1.18 (fixed)
$C_{D_{\alpha 3}}$	-0.81 (fixed)	-0.66 (fixed)
	Lift	
C_{L_0}	0.346 ± 0.011	0.319 ± 0.011
C_{L_α}	-0.67 ± 0.12	-0.58 ± 0.12
$C_{L_{\alpha 2}}$	-1.05 (fixed)	-1.02 (fixed)
$C_{L_{\alpha 3}}$	0.75 (fixed)	0.85 (fixed)
	Moment	
α_{trim}, deg	$+0.1 \pm 0.2$	-1.3 ± 0.4
C_{M_α}	-0.129 ± 0.001	-0.143 ± 0.002
$C_{M_{\alpha 2}}$	-0.045 (fixed)	-0.047 (fixed)

the stagnation pressure was about 2, and the corrections to the aerodynamic coefficients are

$$\Delta C_D = -0.08 - 0.02 \sin\alpha + 0.04 \sin^2\alpha + \cdots$$

$$\Delta C_L = -0.02 + 0.08 \sin\alpha + 0.01 \sin^2\alpha + \cdots$$

$$\Delta C_M = 0.003$$

For the HFFAF runs the higher-order terms could not be determined because of two factors: the limitation on the number of data sets and the accuracy of the measurements. If there are multiple runs with varying amplitudes in the motion, the higher-order terms can be calculated. However, if there is only one run, the higher-order terms introduce only small perturbations to the motion described by a truncated expansion of the aerodynamic coefficients. To further compound the problem, the orientation and position measurements are less accurate than is typical for the HFFAF. The angle measurements are accurate to ± 0.5 deg, rather than the usual 0.1 deg; the position measurements are accurate to ± 0.02 in., rather than 0.001 in. These errors are caused by difficulties in measuring the orientations and positions of blunt models in ballistic range shadowgraphs. New advances in computerized film reading[25] should greatly reduce these errors.

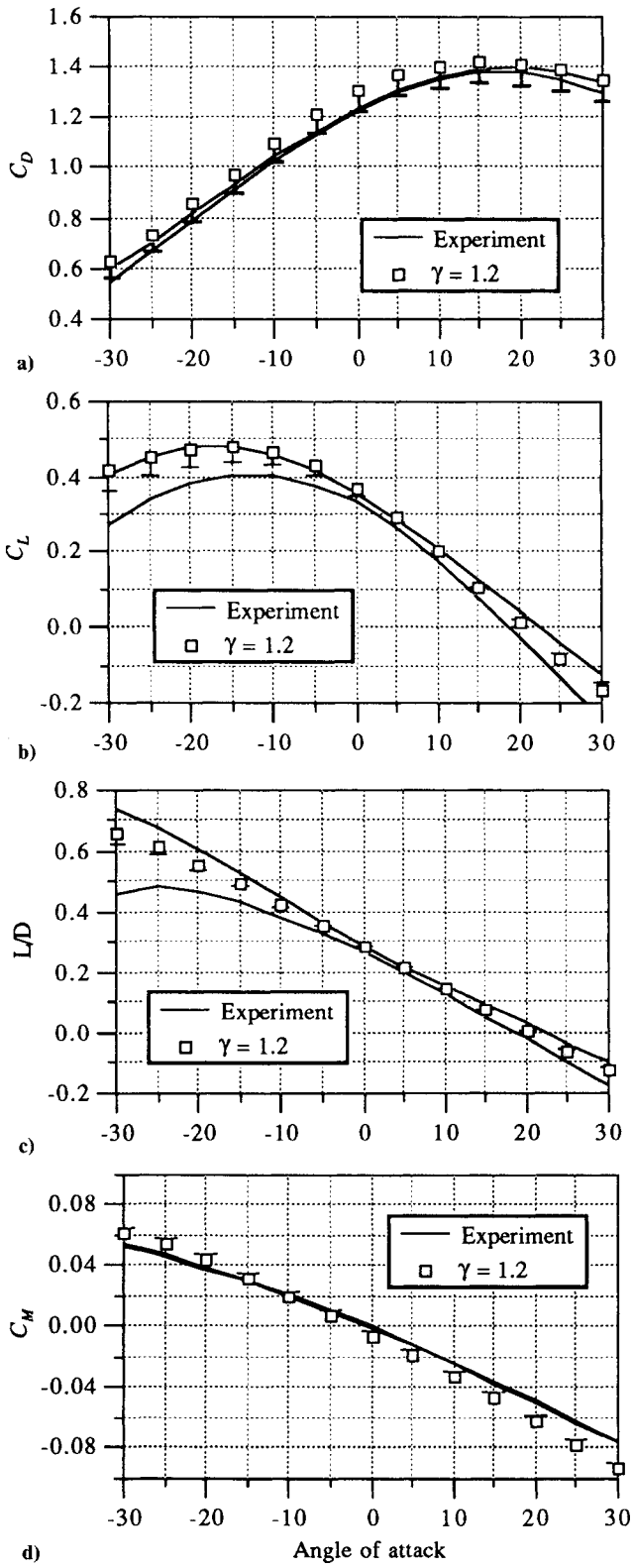

Fig. 7 Aerodynamic coefficients for run 1700.

However, with one experimental data set there is enough information to calculate the two lowest-order terms in the lift, drag, and moment coefficients for models with minimal roll; the second- and third-order terms were fixed to their CFD values plus the estimated correction from the base. First-order terms for the side force and yawing motions were also calculated; however, there was too little information available to obtain higher-order terms, especially since the rolling of the models masked their effects.

The experimental coefficients are given in Table 3, and the experimental results are plotted in Figs. 7 and 8. The squares represent the computed values from the forebody solution; the hash marks give the approximated values with base flow corrections. The solid lines give the upper and lower estimates for the experimental aerodynamic coefficients. As indicated by these upper and lower bounds, the moment coefficients can be determined very accurately with two cycles of motion. The drag can also be accurately determined. The lift coefficient has the largest amount of error. In general, lift is the most difficult aerodynamic coefficient to measure in the HFFAF, and if the CFD values for the higher-order terms in the expansion of the lift coefficient are incorrect, the errors are magnified.

The experimental and computed drag and lift coefficients for run 1700 show good agreement, expecially when the base corrections have been included. The experimental drag coefficient lies between the CFD forebody value and the forebody value plus base correction. The computed lift plus base correction lies in the center of the upper and lower estimates for the experimental lift. The first two terms in the expansions of the experimental and computed drag and lift coefficients also show good agreement when the base flow corrections have been added to the computed values.

For run 1701 the agreement between the experimental and computed drag and lift coefficients is not as good. The experimental drag is larger than its computed value, and the experimental lift is lower. Some of these differences are attributable to the rolling and yawing of the model. With only one data set, errors in calculating the yawing moment, side forces, and roll rates can introduce errors into the drag and lift calculations. These errors are minimized when multiple sets of data are used in the data analysis procedure. Since the computations indicated that the drag and lift coefficients had only a small dependency on Mach number in the range of 9.2–11.8, these coefficients were found simultaneously for runs 1700 and 1701. The results are shown in Fig. 9.

The use of multiple data sets did significantly improve the agreement between the experimental and computed drag coefficients, and the experimental error band was reduced from that obtained with the run 1701 case alone. The error band for the experimental lift coefficient is still large, and there are some differences between experiment and computation at negative angles of attack; however, the fit is now quite good for positive angles of attack. There is still not enough information to separate out the effects of the side and lift forces on the motion of rolling models, and the yaw and roll may be contributing to the pitching motion. Additional experimental data sets are necessary to further refine the experimental lift coefficient.

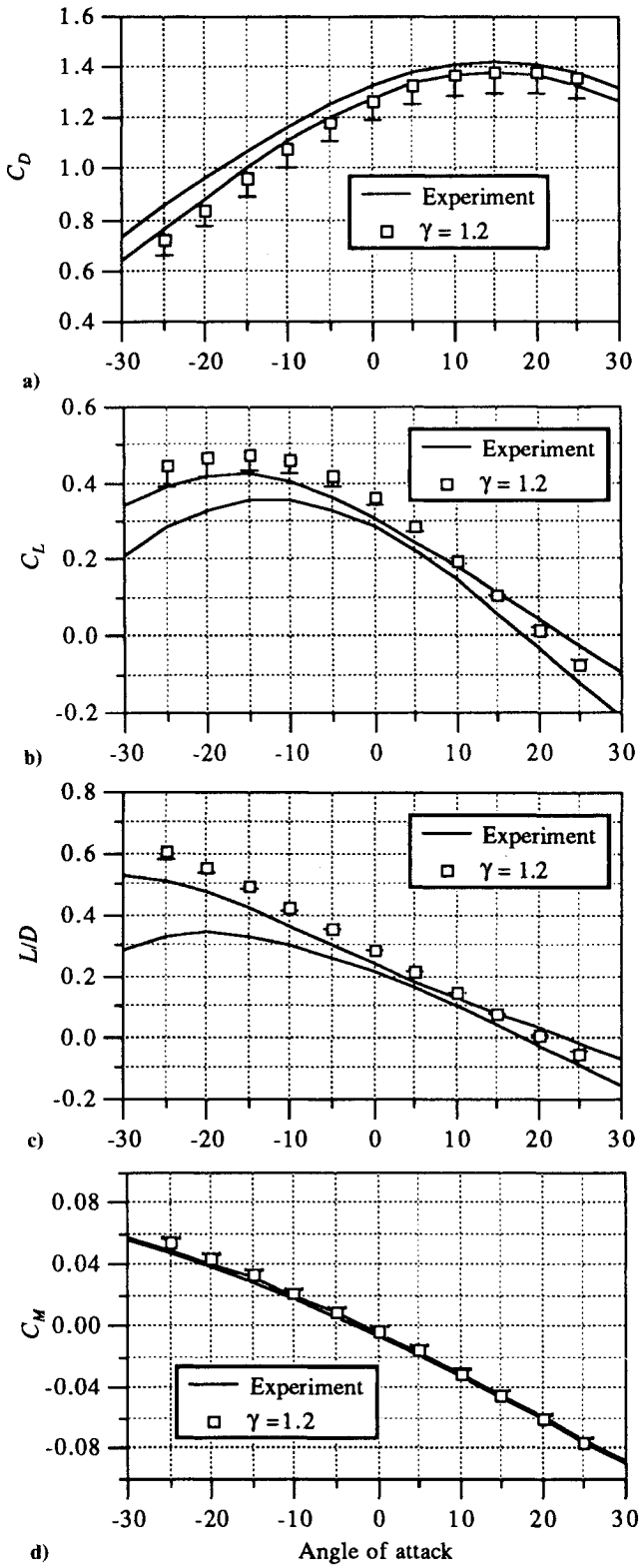

Fig. 8 Aerodynamic coefficients for run 1701.

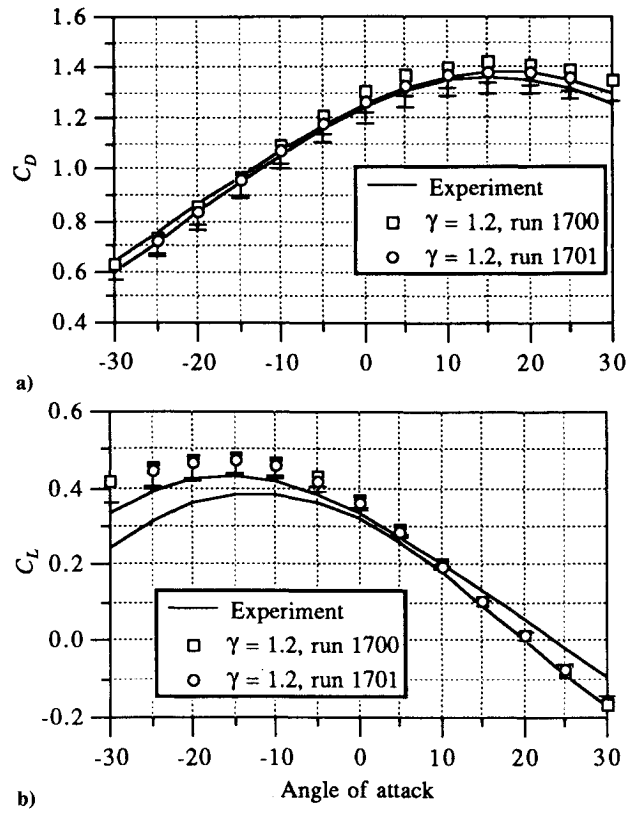

Fig. 9 Drag and lift coefficients for combined runs.

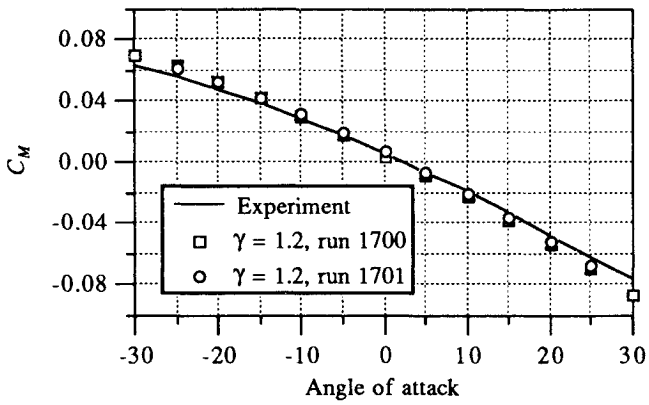

Fig. 10 Moment coefficient at design center of gravity.

The experimental pitching moment coefficient for run 1700 does show some deviation from the computed coefficient, whereas there is little deviation in the run 1701 case. As shown in Eqs. (10) and (11), the moment forces are proportional to the moments of inertia; for these models it is difficult to accurately measure the moments of inertia, and there may be a constant multiplier contributing to the differences between the experimental and computed moment coefficients. However, this constant should have only a small effect on the trim angle. In addition, there may be some corrections from small errors in the measured center-of-gravity location.

The center of gravity for the HFFAF models was offset from the vehicle design center of gravity. This does introduce a correction to the moment coefficient. The moment coefficient at the design center of gravity is given by

$$C_M(\text{design center}) = C_M - [C_L \cos\alpha + C_D \sin\alpha]\Delta x/l - [C_D \cos\alpha - C_L \sin\alpha]\Delta z/l$$

where Δx and Δz give the displacement from the model center of gravity to the design center of gravity in the coordinate system shown in Fig. 4, and l is the diameter of the model. The moment coefficient for the design center of mass is shown in Fig. 10. The experimental value was obtained using multiple sets in the data reduction routine, and both the computed moment coefficients for runs 1700 and 1701 are shown. There is good agreement between the experimental and computed moment coefficients, and the trim angle for the design center of gravity is ~14.7 deg relative to the base plane of the model.

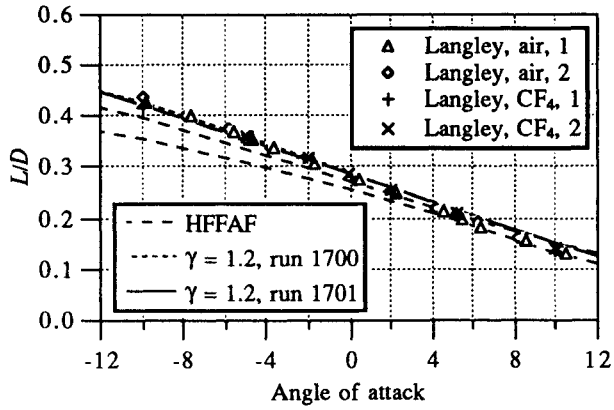

Fig. 11 *L/D* comparison.

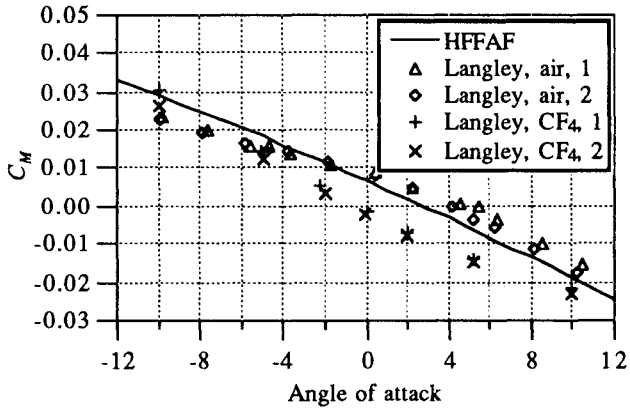

Fig. 12 Moment coefficient comparison.

Comparison to Langley Tunnel Results

In Figs. 11 and 12 the HFFAF experimental and computed lift-to-drag ratios (L/D) and moment coefficients are compared to those obtained in the Langley 31-In. Mach 10 Tunnel and the Langley Hypersonic CF_4 Tunnel.[5] The conditions for the Langley tunnel tests included here are given in Table 4. The test gas in the Langley 31-In. Mach 10 Tunnel was air, and the Mach numbers fell between the two HFFAF values. The pressures, temperatures, and velocities were much lower than those for the HFFAF runs. For the Langley Hypersonic CF_4 Tunnel tests, the Mach numbers, pressures, temperatures, and velocities were all lower than the corresponding HFFAF values. The effective γ values, based on calculated thermodynamic properties behind the shock, were 1.34 for the Langley 31-In. Mach 10 Tunnel tests and 1.11 for the Langley Hypersonic CF_4 Tunnel tests. For the HFFAF runs the shock standoff distance was matched using $\gamma = 1.2$.

The HFFAF experimental results shown in Fig. 11 were obtained using the six-degree-of-freedom data reduction routine with runs 1700 and 1701. As mentioned previously, the rolling and yawing motion did affect the calculated lift coefficient, and the computed L/D does not lie within the upper and lower bounds of the experimental L/D at negative angles of attack. However, the computed L/D is in excellent agreement with all of the Langley results shown here. The effects of Mach number, Reynolds number, and γ on L/D are minimal.

In Fig. 12 the moment coefficients at the design center of gravity are shown for the HFFAF, Langley 31-In. Mach 10 Tunnel, and Langley Hypersonic CF_4 Tunnel tests. The moment coefficients and trim angles for these three cases do not agree. For a wide range of conditions, tests at Langley[5] indicated that the moment coefficient was independent of the Mach number and Reynolds numbers; however, variations in the effective γ had a pronounced effect on the moment coefficient. Computations performed by Micol[24] also indicated a pronounced effect of γ on the forebody pressure distribution. Therefore, the differences in the wind-tunnel and ballistic range results are attributable to variations in γ and, hence, real-gas effects. The curvature of the moment coefficient ($C_{M_{\alpha 2}}$) is negative for the Langley 31-In. Mach 10 Tunnel cases ($\gamma = 1.34$), negative but less so for the HFFAF cases ($\gamma = 1.20$), and positive for the CF_4 cases ($\gamma = 1.11$). The respective trim angles for these three cases are 12, 14.7, and 17 deg.

Table 4 Experimental conditions for Langley tunnel tests

Test	Pressure, Torr	Temperature, K	Velocity, km/s	Mach number	Model diam, in.
Air, 1	0.9	51	1.42	9.9	2.50
Air, 2	1.7	50	1.43	10.05	3.67
CF_4, 1	1.3	167	0.87	6.28	2.50
CF_4, 2	2.0	162	0.87	6.10	3.67

Conclusions

The use of a combination of experiment and CFD has proven effective in the interpretation of free-flight data. In this study of the AFE trim angle, sufficient free-flight data were not available for calculating higher-order terms in the series expansions of the aerodynamic coefficients. To extract information from the experimental data, the curvature of the function describing the moment coefficient had to be known, and this was provided by CFD. In the analysis of the HFFAF data, the higher-order terms in the aerodynamic coefficient expansions were set equal to the CFD values; the lower-order terms were found using a six-degree-of-freedom, weighted, least-squares procedure. The resulting experimental and CFD aerodynamic coefficients and trim angles are in good agreement.

Comparison of the HFFAF and Langley tunnel results shows a strong dependency of the moment coefficient and trim angle on real-gas effects. All three facilities had different effective specific heat ratios: 1.34 for the Langley 31-In. Mach 10 Tunnel, 1.2 for the test conditions in the HFFAF, and 1.11 for the Langley Hypersonic CF_4 Tunnel. The trim angles found in these three facilities were, respectively, 12, 14.7, and 17 deg. The trim angle was sensitive to the effective specific heat ratio, and to accurately predict the trim angle at flight conditions, the state of the gas must be correctly modeled.

This is important for the AFE. In the current design the trajectory and angle of attack are controlled by reaction control systems, and the radiation from particular regions of the wake flow is measured by rearward-viewing radiometers. Better knowledge of the trim angle and its uncertainty will reduce the amount of fuel required by the reaction control systems and reduce the uncertainty in the radiometer specifications. By use of a combination of CFD studies and ground-based experiments, the real-gas effects at flight conditions can be modeled and the estimates of the trim angle can be improved.

In many cases the HFFAF can be used to simulate actual flight conditions, and reasonable predictions of the moment coefficients and trim angles can be obtained in this facility. Furthermore, the agreement shown here between the experimental and computed results indicates that for blunt bodies, such as the AFE, at these test conditions, the moment coefficients and trim angles can be computed using efficient ideal-gas solvers with an appropriate choice of the specific heat ratio. The appropriate specific heat ratio can be found from real-gas CFD solvers or from shock-shape comparisons. In cases where the actual flight conditions cannot be duplicated in ground-based facilities, real-gas solvers must be used to check the validity of using ideal-gas solvers with constant specific heat ratios to predict moment coefficients and trim angles. At flight conditions, variations in the specific heat ratio may have sizable effects on the moment coefficients and trim angles.

Acknowledgments

Support for L. A. Yates and E. Venkatapathy was provided by NASA Grants NCC2-583 and NCC2-420. We wish to thank Dinesh Prabhu for supplying us with a code for calculating aerodynamic coefficients from flowfield solutions.

References

[1]Weilmuenster, K. J., and Gnoffo, P. A., "Aeroassisted Flight Experiment Aerodynamic Characteristics at Flight Conditions," *Journal of Spacecraft and Rockets,* Vol. 27, No. 6, 1990, pp. 684–686.

[2]Weilmuenster, K. J., and Hamilton, H. H., III, "A Comparison of Computed and Measured Aerodynamic Characteristics of a Proposed Aeroassist Experiment Configuration," NASA TM 89034, Jan. 1987.

[3]Park, C., and Yoon, S., "Calculation of Real-Gas Effects on Blunt-Body Trim Angles," AIAA Paper 89-0685, Jan. 1989.

[4]Intrieri, P. F., and Kirk, D. B., "High-Speed Aerodynamics of Several Blunt-Cone Configurations," *Journal of Spacecraft and Rockets,* Vol. 24, No. 2, 1987, pp. 127–132.

[5]Wells, W. L., "Measured and Predicted Aerodynamic Coefficients and Shock Shapes for the Aeroassist Flight Experiment (AFE) Configuration," NASA TP 2956, Jan. 1990.

[6]Cheatwood, F. M., DeJarnette, F. R., and Hamilton, H. H., III, "Geometrical Description for a Proposed Aeroassist Flight Experiment Vehicle," NASA TM 87714, July 1986.

[7]Etkin, B., *Dynamics of Atmospheric Flight,* Wiley, New York, 1972, pp. 104–152.

[8]Chapman, G. T., and Kirk, D. B., "A Method for Extracting Aerodynamic Coefficients from Free-Flight Data," *AIAA Journal,* Vol. 8, No. 4, 1970, pp. 753–758.

[9]Chapman, G. T., Kirk, D. B., and Malcolm, G. N., "Aerodynamics of Bodies from Motion Analysis," *Ballistic Range Technology,* edited by T. N. Canning, A. Seiff, and C. S. James, AGARDograph 138, Aug. 1970.

[10]Palmer, G., "Enhanced Thermochemical Nonequilibrium Computations for Flow Around the Aeroassist Flight Experiment Vehicle," AIAA Paper 90-1702, June 1990.

[11]Gnoffo, P. A., "A Code Calibration Program in Support of the Aeroassist Flight Experiment," AIAA Paper 89-1673, June 1989.

[12]Venkatapathy, E., Feiereisen, W. J., and Obayashi, S., "Computational Studies of Hard-Body and 3-D Effects in Plume Flows," AIAA Paper 89-0129, Jan. 1989.

[13]Obayashi, S., "Numerical Simulation of Underexpanded Plumes Using Upwind Algorithms," AIAA Paper 88-4360, Oct. 1988.

[14]Venkatapathy, E., "Computational Results for 2-D and 3-D Ramp Flows with an Upwind Navier-Stokes Solver," *Proceedings of the Workshop on Hypersonic Flows for Reentry Problems,* Springer-Verlag, New York (to be published).

[15]Ruffin, S. M., Venkatapathy, E., Keener, E. R., and Nagaraj, N., "Computational Aspects of a NASP Nozzle/Afterbody Experiment," AIAA Paper 89-0446, Jan. 1989.

[16]Palmer, G., and Venkatapathy, E., "Effective Singular Line Boundary Conditions for Three-Dimensional Grids," AIAA Paper 92-0545, Jan. 1992.

[17]Lomax, H., and Inouye, M., "Numerical Analysis of Flow Properties about Blunt Bodies Moving at Supersonic Speeds in an Equilibrium Gas," NASA TR R-204, July 1964.

[18]Tokarcik, S., Venkatapathy, E., Palmer, G., and Candler, G., "Computational Flow Predictions for Hypersonic Ballutes," AIAA Paper 91-3303, Sept. 1991.

[19]Jones, R. A., and Hunt, J. L., "Measured Pressure Distributions on Large-Angle Cones in Hypersonic Flows of Tetrafluoromethane, Air, and Helium," NASA TN D-7429, Dec. 1973.

[20]Jorgensen, L. H., "Charts of Isentropic Exponent as a Function of Enthalpy for Various Gases in Equilibrium," NASA SP 3020, 1965.

[21]Davies, C. B., and Venkatapathy, E., "Application of a Solution-Adaptive Grid Scheme, SAGE, to Complex Three-Dimensional Flows," AIAA Paper 91-1594, June 1991.

[22]Miller, C. G., III, "Shock Shapes on Blunt Bodies in Hypersonic-Hypervelocity Helium, Air, and CO2 Flows, and Calibration Results in Langley 6-Inch Expansion Tube," NASA TN D-7800, Feb. 1975.

[23]Venkatapathy, E., Palmer, G., and Prabhu, D., "AFE Base Flow Computations," AIAA Paper 91-1372, June 1991.

[24]Micol, J. R., "Simulation of Real-Gas Effects on Pressure Distributions for a Proposed Aeroassist Flight Experiment and Comparison to Prediction," AIAA Paper 87-2368, 1987.

[25]Yates, L. A., "Improved Accuracy in Ground-Based Facilities—Development of an Automated Film-Reading System for Ballistic Ranges," 17th AIAA Ground Testing Conference, AIAA Paper 92-4000, July 1992.

Ernest V. Zoby
Associate Editor